



# High-dimensional angular two-photon interference and angular qudit states

GRACIANA PUENTES<sup>1,2,3,\*</sup> 

<sup>1</sup>Universidad de Buenos Aires, Facultad de Ciencias Exactas y Naturales, Departamento de Física, Buenos Aires (C1078AAI), Argentina

<sup>2</sup>CONICET-Universidad de Buenos Aires, Instituto de Física de Buenos Aires (IFIBA), Buenos Aires C1428BFA, Argentina

<sup>3</sup>University of Latvia, Raina boulevard 19, Riga, LV-1586, Latvia

\*[gpuentes@df.uba.ar](mailto:gpuentes@df.uba.ar)

**Abstract:** Using angular position–orbital angular momentum entangled photons, we propose an experiment to generate maximally entangled states in  $D$ -dimensional quantum systems, the so called qudits, by exploiting correlations of parametric down-converted photons. Angular diffraction masks containing  $N$  angular slits in the arms of each twin photon define a qudit space of dimension  $N^2$ , spanned by the alternative pathways of the photons. Numerical results for  $N$  angular slits with  $N = 2, 4, 5, 10$  are reported. We discuss relevant experimental parameters for an experimental implementation of the proposed scheme using Spatial Light Modulators (SLMs), and twin-photons produced by Spontaneous Parametric Down Conversion (SPDC). The entanglement of the qudit state can be quantified in terms of the Concurrence, which can be expressed in terms of the visibility of the interference fringes, or by using Entanglement Witnesses. These results provide an additional means for preparing entangled quantum states in high-dimensions, a fundamental resource for quantum simulation and quantum information protocols.

© 2020 Optical Society of America under the terms of the [OSA Open Access Publishing Agreement](#)

## 1. Introduction

Over the past decades Spontaneous Parametric Down Conversion (SPDC) has become a fundamental process for generation of entangled photonic states. The inherent characteristics of the phenomenon allows the construction of quantum states entangled in many degrees of freedom, such as position and momentum, polarization, time and energy, or angular position and orbital angular momentum (OAM), and provides for a key resource in experimental studies in quantum communications, quantum information, and in fundamentals of quantum mechanics. Entanglement of down-converted photons in a given domain, gives rise to interference effects in that particular domain, as a results of two-photon coherence. Interference effects in twin photons have been observed both in the spatial and temporal domains [1–8]. These effects are customarily used to test the fundamental aspects of quantum physics [9–11] and are a key element to many quantum information protocols such as quantum cryptography and quantum teleportation [12–14]. Fourier relationship linking angular position and OAM leads to angular interference in the OAM-mode distribution of a photon when it passes through an angular aperture, resulting in two-photon interference in the angular domain [15–22].

In this article, we study high-dimensional angular two-photon interference, in a scheme in which entangled photons produced by SPDC are made to pass through multiple angular apertures, in the form of  $N$  angular slits, which results in *path entanglement* in a space of dimension  $D = N^2$ , the so called angular qudits. Using this scheme, it is possible to demonstrate entangled qudit states based on angular-position correlations of down-converted photons. Recently, a remarkable experimental demonstration of high-dimensional entanglement in Orbital Angular Momentum (OAM), corresponding to a Hilbert space of dimension  $D = 13^2 = 169$ , was reported for the first

time via measurements of generalized violations of Bells inequalities [21]. We stress the strong link between the detection basis reported in Ref. [21], and the angular qudit states proposed in our scheme. This suggests that such angular qudit states could possibly be suited for experimental demonstrations of violations of Bells inequalities in even higher dimensions. In addition, the greater simplicity in our interferometric detection scheme seems to indicate that violations of Bells inequalities in even higher dimensions could in principle be achieved.

While previous approaches [16,17] rely only on the Fourier relation, our manuscript instead shines light on the quantum interpretation, which provides a new insight. In addition, while [23] considers only  $N = 2$  angular slits, here we consider the general case of arbitrary  $N$  angular slits, which can produce high-dimensional entanglement. To this end, we introduce a different generic notation in order to derive theoretical expressions in this context. Moreover, as opposed to previous works, we provide a representation of quantum states in terms of quantum density matrix operators, which further enhances our quantum approach. Adding to the novelty of our work, we consider the case of asymmetric angular slits  $N$  and  $M$  for signal and idler, which can lead to high dimensional interference for mixed states. We note that linear qudits have been previously proposed [24], while here we propose angular qudits. The advantage of angular qudits being that due to their shape they can enable implementations in a larger Hilbert space than linear qudits (see Section IV). Finally, as opposed to previous qubit cases [23,25], in order to quantify entanglement, we propose other alternative entanglement measures such as Logarithmic Negativity, in addition to the Concurrence. For all these reasons, our work shines light into several novel aspects of angular diffraction using single photons.

Entangled two-qubit states are the necessary ingredients for many quantum information protocols [12–14], and they have previously been realized by exploring the correlations of entangled photons in variables including polarization [26], time bin [4,6], frequency [27], position [7,8], transverse momentum [28,29], and OAM [18,20,22]. To date, angular-position correlations of twin photons have only been demonstrated for  $N = 2$  angular slits [23], which represent a two-qubit system. The results presented here extended this notion to an arbitrary number of angular slits  $N$ , which not only demonstrates two-photon coherence effects in the angular domain but also provide an additional means for preparing entangled quantum states in a high-dimensional space (qudits), which is a fundamental resource for quantum information protocols.

The article is organized as follows, in Section I, we present an introduction to the problem and the analytical tools for characterizing high-dimensional interference effects in the angular position-OAM domain. Second, in Section II, we present a numerical representation of typical density matrices of pure maximally entangled states for  $N = 2, 4, 5, 10$ , and we numerically reproduce the results obtained by Jha *et al.*, PRL 2010 [23] for the case  $N = 2$  (see Appendix A). In Section III, we present numerical results for multi-path interference effects for  $N > 2$  angular slits, and for the case of an asymmetric configuration of angular slits  $N = 6$  and  $M = 3$ , resulting in mixed states in a Hilbert space of dimension  $D = 18$ . Next, in Section IV we briefly introduce a scheme based on Entanglement Witnesses to estimate a lower bound on the entanglement content of angular qudits, using the Logarithmic Negativity as a measure of entanglement, which can be applied to generic mixed states. In Section V, we discuss the requirements for an experimental implementation of this proposal, and we provide an estimation of the largest qudit space that can in principle be implemented with this approach using state-of-the-art Spatial Light Modulators. Finally, in Section VI we present our conclusions.

Let us consider the experimental setup described in Fig. 1(a). In the simplest scenario, a Gaussian pump beam produces signal ( $s$ ) and idler ( $i$ ) entangled photons by the non-linear process of SPDC. For a Gaussian pump beam with zero OAM ( $l = 0$ ), phase matching conditions

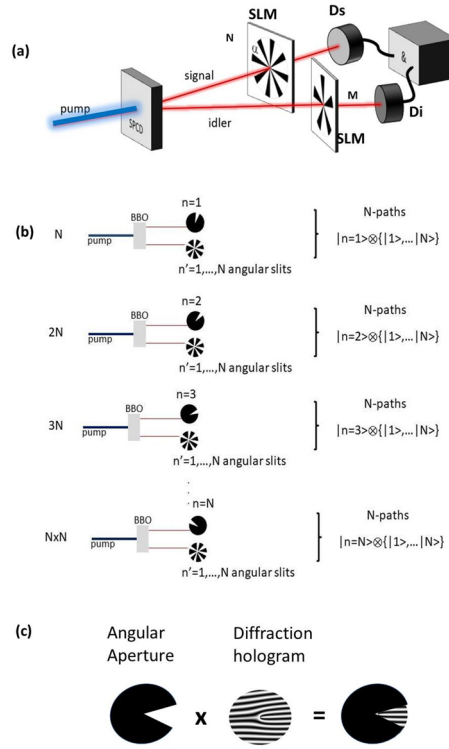


**Fig. 1.** (a) Schematic of proposed experimental setup (see text for details). (b) Two-photon multiple-path diagram showing  $N^2$  alternative paths using angular masks containing  $N$  slits of width  $\alpha$  and separation  $\beta$ , with  $N(\alpha + \beta) \leq 2\pi$ . (c) Angular apertures used to create path-entanglement, and diffraction holograms used to analyze the OAM spectrum. Both the angular aperture and the diffraction hologram are programmed using standard Spatial Light Modulators.

determine that the two-photon down-converted state  $|\psi_{sl}\rangle$  can be expressed as [56]:

$$|\psi_{sl}\rangle = \sum_{l=-\infty}^{+\infty} a_l |l\rangle_s | -l\rangle_i, \quad (1)$$

where  $s$  and  $i$  label signal and idler photons, respectively, and  $|l\rangle$  correspond to OAM eigen-modes of order  $l$ . Such OAM are characterized by an azimuthal phase front expressed as  $e^{il\phi}$ . The coefficients  $|a_l|^2$  represent the probability of generating photon pairs in an OAM eigen-mode of order  $l$ . In order for  $|\psi_{sl}\rangle$  to represent a quantum state it should be normalized. The normalization condition imposes  $\sum_{l=-\infty}^{+\infty} |a_l|^2 = 1$ . Consequently, signal and idler photons transmitted through  $N$  angular slits, as shown in Fig. 1(a) and Fig. 1(c). The angular slits are placed in the image planes of the crystal. The transmission functions  $A_{j,n}$  of the individual angular slits are given by:

$$A_{j,n}(\phi_j) = 1 \text{ if } n\beta - \alpha/2 \leq \phi_j \leq n\beta + \alpha/2 \text{ else } 0, \quad (2)$$

where  $j = (s, i)$  is the label for signal and idler, and  $n = 0, \dots, N - 1$  is the angular slit label. Here  $\alpha$  represents the aperture of the angular slits, and  $\beta$  represents the separation between consecutive angular slits (see Fig. 1(b)). Note that our notation can enable to obtain a compact expression even for the case of  $N$  angular slits. For the simplest scenario  $N = 2$  slits, we recover the results presented in Jha *et al.* PRL 2010 [23]. Therefore, there are in principle  $N^2$  alternative pathways,

represented by the two-photon path diagrams described in Fig. 1(b), by which the down-converted photons can pass through the apertures and get detected in coincidence at single-photon avalanche detectors  $D_s$  and  $D_i$ . The  $N^2$  alternative paths here labelled by the index  $q = 1, \dots, N^2$ , can be expressed as the tensorial product of the subspaces corresponding to each photon ( $s, i$ ) passing through the slits  $n = 0, \dots, N - 1$ , respectively, in the form:

$$\begin{aligned} &|s, 0\rangle \otimes \{|i, 0\rangle, |i, 1\rangle, \dots, |i, N - 1\rangle\}; \\ &|s, 1\rangle \otimes \{|i, 0\rangle, |i, 1\rangle, \dots, |i, N - 1\rangle\}; \dots \\ &|s, N - 1\rangle \otimes \{|i, 0\rangle, |i, 1\rangle, \dots, |i, N - 1\rangle\}. \end{aligned} \tag{3}$$

Due to the strong correlation between the position of the two photons in the image plane of the crystal, only paths of the form  $|i, n\rangle|s, n\rangle$  will have a significant contribution [23]. We note that in a realistic experimental situation, this assumption may not remain true when  $N$  is too large, due to the finite angular-correlation width of the signal and idler photons. Such limited angular-correlation width will in turn impose fundamental limitations on the maximum number of angular slits  $N$  that can be experimentally implemented. This point is discussed in detail in Section 4 - Proposed Experimental Implementation.

Following the notation introduced in [23], the density matrix operator of the qudit state can be expressed in the following form:

$$\hat{\rho} = \sum_{n=0}^{N-1} \sum_{m=0}^{N-1} \rho_{nm} |s, n\rangle |i, n\rangle \langle s, m| \langle i, m|, \tag{4}$$

where the subindices ( $n = 0, \dots, N - 1$ ) and ( $m = 0, \dots, N - 1$ ) label the angular slits for each photon, and the normalization condition imposes  $\text{Tr}[\hat{\rho}] = \sum_{n=0}^{N-1} \rho_{nn} = 1$ . The off-diagonal terms  $\rho_{nm}$  are complex numbers and can be conveniently expressed as  $\rho_{nm} = \sqrt{\rho_{nn}\rho_{mm}}\mu e^{i\theta}$  [23], where  $\mu$  is the degree of coherence and  $\theta$  is the argument of the coefficient  $\rho_{nm}$ . Due to Hermiticity of the density matrix, we have  $\rho_{nm} = \rho_{mn}^*$ . We note that the degree of coherence  $\mu$  is less than unit for mixed states. For a pure states  $\mu$  is identically equal to one.

We can write the density matrix  $\hat{\rho}$  in the OAM basis by taking the Fourier transform of the amplitude transmissions for the angular slits  $A_{j,n}$ , where ( $j = s, i$ ) is the photon label and ( $n = 0, \dots, N - 1$ ) the slit index, as expressed in Eq. (2). For a given path  $n$ , the two-photon state in the OAM mode basis can be expressed as [23]:

$$\begin{aligned} |s, n\rangle |i, n\rangle &= C \sum_l c_l \sum_{l'} \frac{1}{2\pi} \int_{-\pi}^{\pi} d\phi_s A_{s,n}(\phi_s) e^{-i(l'-l)\phi_s} |l'\rangle \\ &\times \sum_{l''} \frac{1}{2\pi} \int_{-\pi}^{\pi} d\phi_i A_{i,n}(\phi_i) e^{-i(l''+l)\phi_i} |l''\rangle, \end{aligned} \tag{5}$$

where  $C$  is a normalization factor to ensure  $\text{Tr}[\hat{\rho}] = 1$ . We evaluate  $|s, n\rangle |i, n\rangle$  by substituting the expressions for  $A_{j,n}(\phi_j)$ . Using the expression for the Fourier transform of the angular amplitude transmission:

$$\begin{aligned} \tilde{A}_{j,n} &= \frac{1}{2\pi} \int_{-\pi}^{\pi} d\phi A_{j,n}(\phi) e^{-il_j\phi} \\ &= \frac{\alpha e^{-il_j\beta n}}{2\pi} \text{sinc}\left(\frac{\alpha}{2} l_j\right), \end{aligned} \tag{6}$$

where  $\text{sinc}(x) = \frac{\sin(x)}{x}$ . The coincidence count rate  $R_{s,i}$  of detectors  $D_i$  and  $D_s$ , gives the probability that a signal photon is detected at detector  $D_s$  in mode  $|l_s\rangle$ , and an idler photon is detected at

detector  $D_i$  in mode  $|l_i\rangle$  in a given fixed time window. It is given by  $R_{si} = \langle l_i | \langle l_s | \hat{\rho} | l_s \rangle_s | l_i \rangle_i$ . Using Eq. (2), Eq. (4) and Eq. (5) we find:

$$R_{si} = \frac{C^2 \alpha^2}{16\pi^4} \left| \sum_{l=-L}^{l=L} c_l \text{sinc}((l_s - l)\alpha/2) \text{sinc}((l_i + l)\alpha/2) \right|^2 \times \sum_{n=0}^{N-1} \sum_{m=0}^{N-1} \rho_{nm} e^{-i\beta(l_s+l_i)(n-m)} \quad (7)$$

For the case of two angular slits ( $N = 2$ ), we recover the expression presented in Jha *et al.* PRL 2010, however we note that our result is fully generic for the case of arbitrary  $N$  angular slits. In our notation, the two-slit basis results in  $\{|s, 0\rangle |i, 0\rangle, |s, 0\rangle |i, 1\rangle, |s, 1\rangle |i, 0\rangle, |s, 1\rangle |i, 1\rangle\}$ . In this case, the coincidence count rate can be written as:

$$R_{si} = \frac{C^2 \alpha^2}{16\pi^4} \left| \sum_{l=-L}^{l=L} c_l \text{sinc}((l_s - l)\alpha/2) \text{sinc}((l_i + l)\alpha/2) \right|^2 \times [\rho_{00} + \rho_{11} + 2\sqrt{\rho_{00}\rho_{11}}\mu \cos(\beta(l_s + l_i) + \theta)], \quad (8)$$

with  $\text{Tr}[\rho] = \rho_{00} + \rho_{11} = 1$ ,  $\rho_{01} = \sqrt{\rho_{00}\rho_{11}}\mu e^{i\theta}$ , and  $\rho_{10} = \sqrt{\rho_{00}\rho_{11}}\mu e^{-i\theta}$ .

The diffraction due to the angular apertures  $\alpha$  is described by the diffraction envelopes of the form  $|\sum_{l=-L}^{l=L} c_l \text{sinc}((l_s - l)\alpha/2) \text{sinc}((l_i + l)\alpha/2)|^2$ . On the other hand, the multi-path interference term only depends on the separation between slits  $\beta$ , and is given by the multiple interference term:

$$\sum_{n=0}^{N-1} \sum_{m=0}^{N-1} \rho_{nm} e^{-i\beta(l_s+l_i)(n-m)}. \quad (9)$$

By measuring such high order interference fringes, via coincidence detection, we can demonstrate entanglement in a high-dimensional space of dimension  $D = N^2$ .

For a two-level system, the visibility  $V$  of the interference pattern is quantified by the off-diagonal terms:

$$V = 2\sqrt{\rho_{00}\rho_{11}}\mu, \quad (10)$$

we note that this expression for the visibility is valid only for the specific class of pure states or partially mixed states described by the density matrix in Eq. (4). For general mixed states the visibility should not take a single expression, it should depend on all off-diagonal elements of the form  $\rho_{nm,n'm'}$  (see Eq. (12) for further details).

For a two qubit system ( $N = 2$ ), the entanglement can be characterized in terms of the Concurrence [30], given by  $C = \max\{0, \lambda_1, \lambda_2, \lambda_3, \lambda_4\}$ , where  $\lambda_i$  ( $i = 1, 2, 3, 4$ ) are the positive eigen-values in descending order of the operator  $R$ , with  $R^2 = \sqrt{\rho}\sigma_y \otimes \sigma_y \rho^* \sigma_y \otimes \sigma_y \sqrt{\rho}$ , where  $\sigma_y$  is a Pauli matrix. For the density matrix in Eq. (4), the Concurrence results equal to the visibility ( $V$ ) of the angular two-photon interference fringes  $C = V = 2\sqrt{\rho_{00}\rho_{11}}\mu$ . We stress that this relation between Concurrence and visibility ( $C = V$ ) is valid only for two qubit systems ( $N = 2$ ).

For the multi-path interference case ( $N > 2$ ), the entanglement content can be estimated using Logarithmic Negativity, via an Entanglement Witness protocol, as discussed in Section IV.

### 1.1. Asymmetric slit number

We now consider the more general case of an asymmetric number of slits  $N$  and  $M$  for signal and idler photons, respectively [24]. For perfectly phase-matched down-converted photons, spatial correlations in the image plane of the crystal determine that signal and idler can only go through opposite slits, and the state of the two photons is a pure maximally-entangled state of the form given in Eq. (4). However, for imperfect phase matching, which can in turn be achieved

via pump engineering [24], signal and idler can go through asymmetric slits  $N$  and  $M$ , and the possible pathways will take the general form  $|s, n\rangle|i, m\rangle$  (with  $n \neq m$ ). This will produce, in turn, non-maximally entangled *pure* states, as reported in Ref. [24].

In a more general scenario, we can consider the generation of non-maximally entangled *mixed* states, by introducing some form of randomness. Several methods have been suggested for generation of photonic mixed-entangled states, for instance by introducing spatial decoherers [31], by adding white noise [32], or by employing incoherent temporal mixing [33], as well as by considering hybrid techniques.

In the OAM representation, the asymmetric pathways for signal ( $s$ ) and idler ( $i$ ) result in:

$$\begin{aligned}
 |s, n\rangle|i, m\rangle = & C \sum_l c_l \sum_{l'} \frac{1}{2\pi} \int_{-\pi}^{\pi} d\phi_s A_{s,n}(\phi_s) e^{-i(l'-l)\phi_s} |l'\rangle \\
 & \times \sum_{l''} \frac{1}{2\pi} \int_{-\pi}^{\pi} d\phi_i A_{i,m}(\phi_i) e^{-i(l''+l)\phi_i} |l''\rangle.
 \end{aligned}
 \tag{11}$$

Since we are not making any particular assumption about the coefficients  $\rho_{nm,n'm'}$ , the two-photon state will be in a generic mixed state of the form

$$\hat{\rho} = \sum_{n,n'=0}^{N-1} \sum_{m,m'=0}^{M-1} \rho_{nm,n'm'} |s, n\rangle|i, m\rangle \langle s, n'| \langle i, m'|,
 \tag{12}$$

with normalization condition  $\text{Tr}[\hat{\rho}] = 1$ , and Hermiticity condition  $\hat{\rho} = \hat{\rho}^\dagger$ .

Using these equations we can derive an expression for the Coincidence Count Rate for generic mixed states (asymmetric case  $N \neq M$ ), of the form:

$$\begin{aligned}
 R_{si} = & \frac{C^2 \alpha^2}{16\pi^4} \left| \sum_{l=-L}^{l=L} c_l \text{sinc}((l_s - l)\alpha/2) \text{sinc}((l_i + l)\alpha/2) \right|^2 \\
 & \times \sum_{n,n'=0}^{N-1} \sum_{m,m'=0}^{M-1} \rho_{nm,n'm'} e^{-i\beta l_s(n-n')} e^{-i\beta l_i(m-m')}
 \end{aligned}
 \tag{13}$$

Note that for the symmetric case  $m = n$  and  $n' = m'$  we recover the expression obtained for the case  $N = M$  (Eq. (7)).

## 2. Numerical results

### 2.1. Density matrix graphical representation

In this Section we present numerical results for the analytical model developed previously. First, we performed graphical representations of the density matrix operator  $\hat{\rho}$  in the complete pathway basis  $\{|s, n\rangle|i, m\rangle\}$  with  $(n, m = 0, \dots, N - 1)$  for pure maximally entangled states. We note that for pure maximally entangled states, the only matrix elements different from zero correspond to states of the form  $\{|s, n\rangle|i, n\rangle\}$ . The diagonal elements satisfy  $\rho_{nn} = \frac{1}{N}$  due to normalization condition, the off-diagonal elements can be expressed as  $\rho_{nm} = \frac{1}{N} e^{i\theta}$ . As reported in Ref. [23], for two-level systems the standard technique to obtain the diagonal elements of the density matrix is via Coincidence Counts. On the other hand, aside from the relative phase  $\theta$ , off-diagonal elements are obtained from the visibility of the interference patterns (see Ref. [23] and References therein, for further details on standard measurement schemes).

In Fig. 2 to Fig. 5, we display a graphical representation of density matrices  $\hat{\rho}$  for ideal pure maximally entangled states, for different phase parameters  $\theta = 0$  and  $\theta = \pi/4$  in the complete pathway basis  $\{|s, n\rangle|i, m\rangle\}$ , labeled by the indices  $(n, m)$  with  $(n = 0, \dots, N - 1)$

and  $(m = 0, \dots, N - 1)$ , for a symmetric configuration of slits of dimensions  $N = 2, 4, 5, 10$ , respectively.  $\text{Re}[\hat{\rho}]$  is displayed on the left column and  $\text{Im}[\hat{\rho}]$  is displayed on the right column. Figures 2(a) and 2(b) ( $N = 2$ ), correspond to diagonal elements  $\rho_{nm} = 1/N$  and off-diagonal elements  $\rho_{nm} = \frac{1}{N}e^{i\theta}$ ,  $\theta = 0$ . Figure 2(c) and 2(d) ( $N = 2$ ), correspond diagonal elements  $\rho_{nm} = 1/N$  and off-diagonal elements  $\rho_{nm} = \frac{1}{N}e^{i\theta}$ , with  $\theta = \pi/4$ . Next, Figs. 3(a) and 3(b) ( $N = 4$ ), correspond to diagonal elements  $\rho_{nm} = 1/N$  and off-diagonal elements  $\rho_{nm} = \frac{1}{N}e^{i\theta}$ , with  $\theta = 0$ , while Fig. 3(c) and 3(d) ( $N = 4$ ), correspond to diagonal elements  $\rho_{nm} = 1/N$  and off-diagonal elements  $\rho_{nm} = \frac{1}{N}e^{i\theta}$ , with  $\theta = \pi/4$ . Figures 4(a) and 4(b) ( $N = 5$ ), correspond to diagonal elements  $\rho_{nm} = 1/N$  and off-diagonal elements  $\rho_{nm} = \frac{1}{N}e^{i\theta}$ ,  $\theta = 0$ , while Fig. 4(c) and 4(d) ( $N = 5$ ), correspond to diagonal elements  $\rho_{nm} = 1/N$  and off-diagonal elements  $\rho_{nm} = \frac{1}{N}e^{i\theta}$ , with  $\theta = \pi/4$ . Finally, Figs. 5(a) and 5(b) ( $N = 10$ ), correspond to diagonal elements  $\rho_{nm} = 1/N$  and off-diagonal elements  $\rho_{nm} = \frac{1}{N}e^{i\theta}$ ,  $\theta = 0$ , while Fig. 5(c) and 5(d) ( $N = 10$ ), correspond to diagonal elements  $\rho_{nm} = 1/N$  and off-diagonal elements  $\rho_{nm} = \frac{1}{N}e^{i\theta}$ , with  $\theta = \pi/4$ .

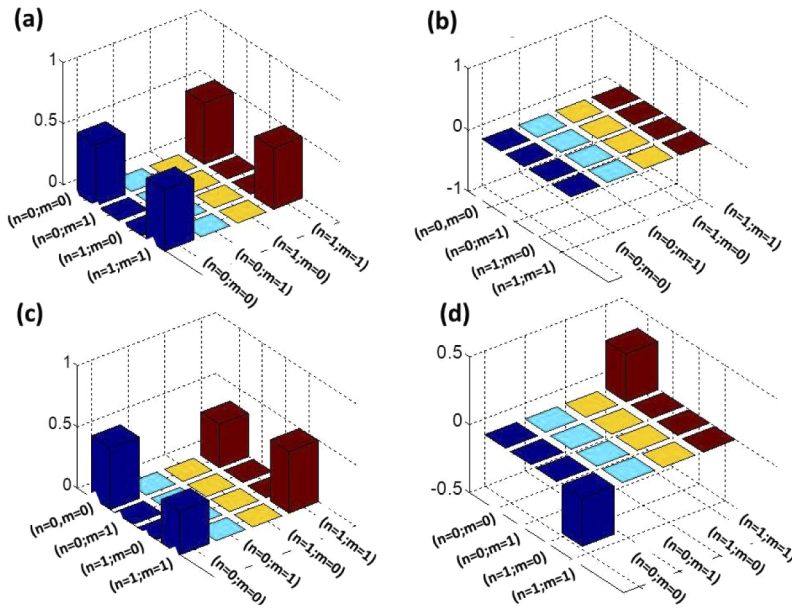


**Fig. 2.** Density matrix representation ( $\hat{\rho}$ ) of pure maximally entangled states, in the complete pathway basis  $\{|s, n\rangle|i, m\rangle\}$  ( $n = 0, \dots, N - 1; m = 0, \dots, N - 1$ ), with  $N = 2$  (see text for details). Left column  $\text{Re}[\hat{\rho}]$ , right column  $\text{Im}[\hat{\rho}]$ , (a)  $N = 2$ ,  $\theta = 0$ , (b)  $N = 2$ ,  $\theta = 0$ , (c)  $N = 2$ ,  $\theta = \pi/4$ , (d)  $N = 2$ ,  $\theta = \pi/4$ .

## 2.2. Angular interference for $N > 2$ angular slits

Having verified that our model fully reproduces the experimental results reported in Jha *et al.* PRL2010 for the simple case  $N = 2$  (see Appendix A), we proceed to the multiple-path interference scenario, for  $N > 2$ . Measurement of such higher order interference fringes, as described by Coincidence Count Rates ( $R_{s_i}$ ) given by Eq. (7), can demonstrate path entanglement in high dimensions. We simulated such multi-path interference fringes case, for the cases  $N = 4, 6, 10$ , and  $l_i = 0, 2, -2$ . We consider  $\alpha = \pi/10, \beta = \pi/4, \pi/7, \pi/11, \pi/14$  and off diagonal elements  $\rho_{nm} = \frac{1}{N}e^{i\theta}$ . In all cases the parameters chosen satisfy the condition  $N(\alpha + \beta) \leq 2\pi$ . The multi-path interference effect is characterized by periodic interference patterns, where the characteristic period decreases with  $\beta$ . Due to limited space and visual clarity, we only display results for the case  $N = 6$ .

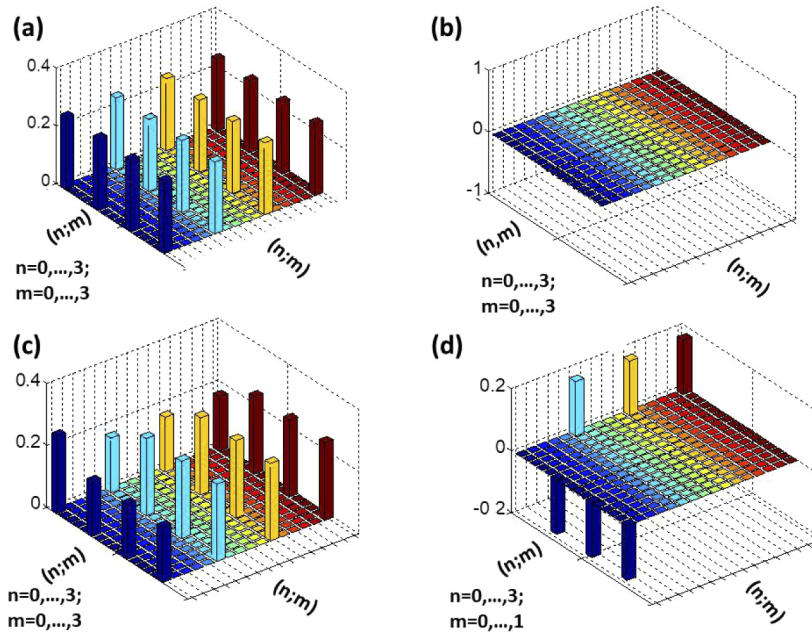


**Fig. 3.** Density matrix representation ( $\hat{\rho}$ ) of pure maximally entangled states, in the complete pathway basis  $\{|s, n\rangle|i, m\rangle\}$  ( $n = 0, \dots, N - 1; m = 0, \dots, N - 1$ ), with  $N = 4$  (see text for details). Left column  $\text{Re}[\hat{\rho}]$ , right column  $\text{Im}[\hat{\rho}]$ , (a)  $N = 4, \theta = 0$ , (b)  $N = 4, \theta = 0$ , (c)  $N = 4, \theta = \pi/4$ , (d)  $N = 4, \theta = \pi/4$ .

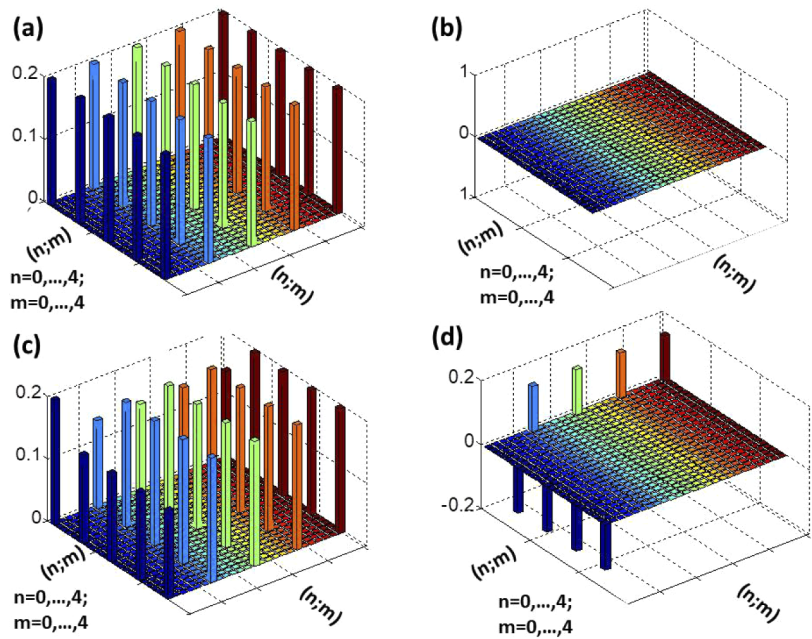


**Fig. 4.** Density matrix representation ( $\hat{\rho}$ ) of pure maximally entangled states, in the complete pathway basis  $\{|s, n\rangle|i, m\rangle\}$  ( $n = 0, \dots, N - 1; m = 0, \dots, N - 1$ ), with  $N = 5$  (see text for details). Left column  $\text{Re}[\hat{\rho}]$ , right column  $\text{Im}[\hat{\rho}]$ , (a)  $N = 5, \theta = 0$ , (b)  $N = 5, \theta = 0$ , (c)  $N = 5, \theta = \pi/4$ , (d)  $N = 5, \theta = \pi/4$ .

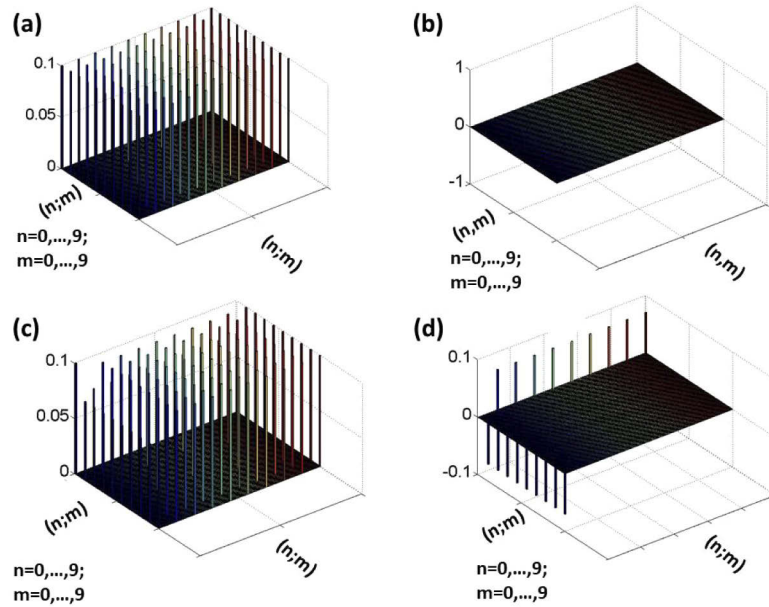


**Fig. 5.** Density matrix ( $\hat{\rho}$ ) representation of pure maximally entangled states in the complete pathway basis  $\{|s, n\rangle|i, m\rangle\}$  ( $n = 0, \dots, N - 1; m = 0, \dots, N - 1$ ), with  $N = 10$  (see text for details). Left column  $\text{Re}[\hat{\rho}]$ , right column  $\text{Im}[\hat{\rho}]$ , (a)  $N = 10, \theta = 0$ , (b)  $N = 10, \theta = 0$ , (c)  $N = 10, \theta = \pi/4$ , (d)  $N = 10, \theta = \pi/4$ .

Figure 6 presents numerical simulations of interference fringes as a function of  $l_s$  (Eq. (7)) for different values of  $l_i$ , and slit separation  $\beta$ , considering  $\alpha = \pi/10$ ,  $\rho_{nm} = \frac{1}{N}e^{i\theta}$ , and  $N = 6$  angular slits, corresponding to a pathway dimension  $D = 36$ . Figure 7(a)  $l_i = -2$ , and Fig. 7(b)  $l_i = 2$ . Figures 7(c)–7(f) display simulated interference fringes, for  $l_i = 0$ ,  $\alpha = \pi/10$ , off-diagonal elements  $\rho_{nm} = \frac{1}{N}e^{i\theta}$ , and different angular separations  $\beta$  of the form: (c)  $\beta = \pi/6$ , (d)  $\beta = \pi/10$ , (e)  $\beta = \pi/12$ , (f)  $\beta = \pi/20$ .

Finally, Fig. 8 displays interference fringes as a function of  $l_s$ , for  $l_i = 0$  and  $\alpha = \pi/10$ , for the case of asymmetric slit number ( $N \neq M$ ). Such non-maximally entangled states could be implemented via imperfect phase matching [24]. We consider  $N = 6$  and  $M = 3$  angular slits, and off diagonal elements  $\rho_{nm} = \frac{1}{\sqrt{NM}}e^{i\theta}$ , for different slit separations  $\beta$ . Such interference effects are a signature of non-maximal path entanglement in a  $D$ -dimensional space spanned by different path alternatives of dimension  $D = N \times M = 18$ . Figure 8(a)  $\beta = \pi/4$ , Fig. 8(b)  $\beta = \pi/7$ . As expected the period of the interference pattern decreases as  $\beta$  increases (see Eq. (13) for details).

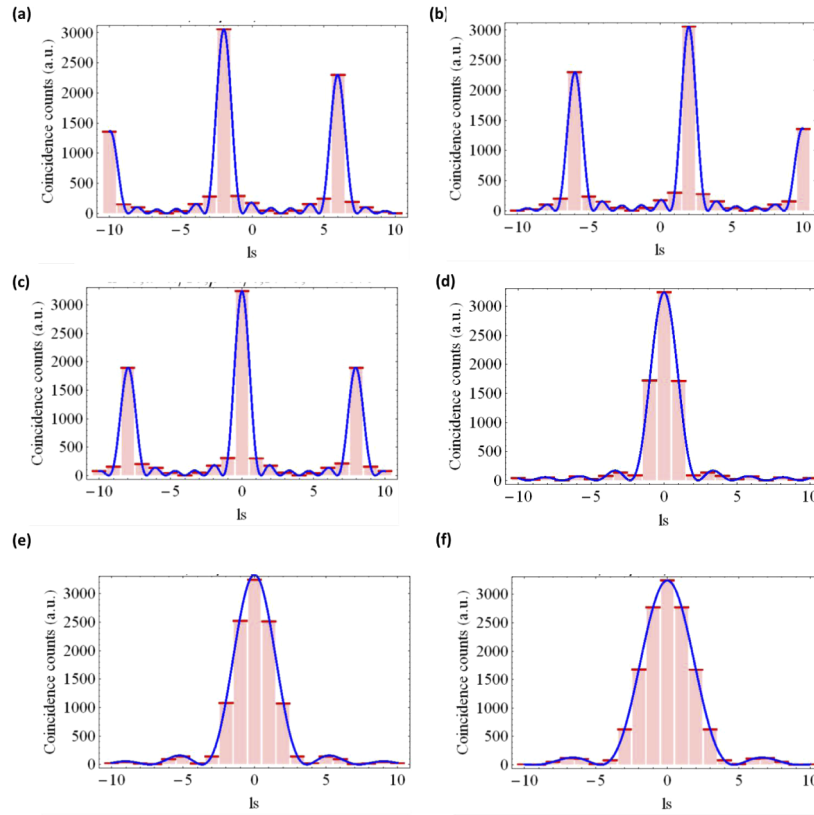


**Fig. 6.** Simulated interference fringes, given by Coincidence Count Rates ( $R_{st}$ ) in Eq. (7), for off diagonal elements  $\rho_{nm} = \frac{1}{N}e^{i\theta}$ ,  $\alpha = \pi/10$ ,  $\beta = \pi/4$ , and  $N = 6$  angular slits. (a)  $l_i = 2$ , (b)  $l_i = -2$ . Due to OAM correlations between twin photons the interference pattern has a maximum for  $l_s = -l_i$ . Figures (c)-(f) correspond to different angular separation  $\beta$ , for  $l_i = 0$  and  $\alpha = \pi/10$ . (c)  $\beta = \pi/4$ , (d)  $\beta = \pi/7$ , (e)  $\beta = \pi/11$ , (f)  $\beta = \pi/14$ . As expected the period of the interference pattern decreases as  $\beta$  increases (see text for details).

### 3. Entanglement witnesses

For the case of  $N = 2$  angular slits, the entanglement content can be easily quantified via the Concurrence [34], in terms of the visibility ( $V$ ) of the interference pattern. Wootters's Concurrence is defined with the help of the super-operator that flips the spin of a qubit. This concept can be generalized to quantum systems of arbitrary dimension, by introducing the corresponding generalized concurrence for joint pure states of bipartite quantum systems, as proposed by Rungta *et al.* [35]. Namely, for a joint pure state  $|\psi_{AB}\rangle$  of a  $D_1 \times D_2$  dimensional bipartite system, the generalized Concurrence is given by:

$$C(\psi_{AB}) = 2\nu_{D1}\nu_{D2}[1 - \text{Tr}(\hat{\rho}_A^2)], \quad (14)$$

where  $\hat{\rho}_A$  is the marginal density operator for system A, and  $(\nu_{D1}, \nu_{D2})$  are positive parameters. We note that this measure of entanglement only applies to pure bipartite states in arbitrary dimensions, and can not be applied for the case of mixed states.

For larger spaces ( $N > 2$ ), and generic mixed entangled states, the amount of entanglement can be estimated via an Entanglement Witness [36]. The advantage of the Entanglement Witness approach is that it does not require full tomographic reconstruction of the density matrix, a highly

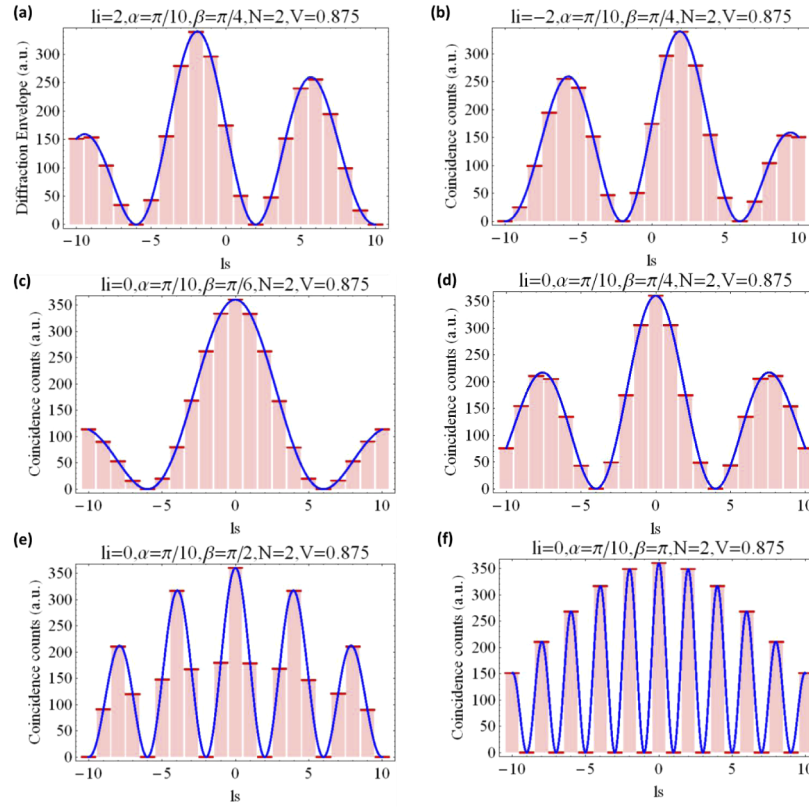


**Fig. 7.** Simulated interference fringes, given by Coincidence Count Rates ( $R_{st}$ ) in Eq. (7), for a reported visibility  $V = 0.875$  [23], and  $N = 2$  angular slits. (a)  $l_i = 2$ , (b)  $l_i = -2$ . Due to OAM correlations between twin photons the interference pattern has a maximum for  $l_s = -l_i$ . Figures (c)-(f) correspond to different angular separation  $\beta$  for  $l_i = 0$  and  $\alpha = \pi/10$ . (c)  $\beta = \pi/6$ , (d)  $\beta = \pi/4$ , (e)  $\beta = \pi/2$ , (f)  $\beta = \pi$ . As expected the period of the interference pattern decreases as  $\beta$  increases (see Eq. (7) for details). Our numerical results fully reproduce the experimental results reported in Ref. [23].

time and resource consuming approach, specially for high-dimensional systems as studied in this article. The problem solved by the Entanglement Witness consists of estimating the least amount of entanglement compatible with a physical density matrix, and with an incomplete set of measurement outcomes. This problem is customarily presented in a compact notations as:

$$E_{\min} = \min_{\hat{\rho}} \{E(\hat{\rho}) : \text{Tr}(\hat{\rho}M_i) = m_i\}, \quad (15)$$

where  $M_i$  are the measurements operators, typically described by a Positive Operator Valued Measurement (POVM), with measurement data  $m_i$ , and  $E$  is a given measure of entanglement. In addition,  $\hat{\rho}$  is required to be positive definite and normalized constraint  $\text{Tr}(\hat{\rho}) = 1$ , in order to represent a physical density matrix. Below, we describe a protocol presented in Refs. [37,38] which enable the Entanglement Witness problem to be solved as a semi-definite program considering that the entanglement measure is the Logarithmic Negativity [39].

For a bipartite system ( $AB$ ), the Logarithmic Negativity is defined as the logarithm of the 1-norm of the partial transposed density matrix  $\|\hat{\rho}^{TA}\|_1$ . The 1-norm can be expressed as [40]

$$\|\hat{\rho}^{TA}\|_1 = \max_{\|H\|_{\infty}=1} \text{Tr}(H\hat{\rho}^{TA}) = \max_{\|H\|_{\infty}=1} \text{Tr}(H^T\hat{\rho}), \quad (16)$$

where the maximization condition is set over all possible Hermitian operators  $H$ , and where  $\|\cdot\|_\infty$  denotes the largest singular value of the matrix.

Since logarithm is a monotonous function, the minimization presented in Eq. (15) can be expressed as

$$\mathcal{N}_{\min} = \log \min_{\hat{\rho}} \{ \max_H \{ \text{Tr}(H^{TA} \hat{\rho}) \mid \|H\|_\infty = 1 \} : \text{Tr}(\hat{\rho} M_i) = m_i \}.$$

This can be expressed as:

$$\mathcal{N}_{\min} = \log \max_H \{ \min_{\hat{\rho}} \{ \text{Tr}(H^{TA} \hat{\rho}) : \text{Tr}(\hat{\rho} M_i) = m_i \} : \|H\|_\infty = 1 \}.$$

For any real numbers  $\{v_i\}$  for which

$$H^{TA} \geq \sum_i v_i M_i. \tag{17}$$

The lower bound on this equation, corresponds to the minimum amount of entanglement compatible with the measurements outcomes  $m_i$  for a physical state  $\hat{\rho}$ , results in:

$$\text{Tr}(H^{TA} \hat{\rho}) \geq \sum_i v_i \text{Tr}(M_i \hat{\rho}) = \sum_i v_i m_i. \tag{18}$$

Finally we arrive at the compact expression:

$$\begin{aligned} \mathcal{N}_{\min} \geq & \log \max_H \{ \\ & \times \max_{v_i} \left\{ \sum_i v_i m_i : H^{TA} \geq \sum_i v_i M_i \right\} : \\ & \|H\|_\infty = 1 \}. \end{aligned} \tag{19}$$

Having defined the measurement operators  $M_i$  any choice of Hermitian operator  $H$  and parameters  $v_i$  such that  $H^{TA} \geq \sum_i v_i M_i$  and  $\|H\|_\infty = 1$ , can provide for a lower bound on the Logarithmic Negativity of states compatible with expectation values of  $m_i$ .

Therefore, we can rewrite Eq. (19) as:

$$\begin{aligned} & \text{maximize} \quad \log \left( \sum_i v_i m_i \right), \\ & \text{subject to} \quad H^{TA} \geq \sum_i v_i M_i, \\ & \text{and} \quad -\mathbb{I} \leq H \leq \mathbb{I}, \end{aligned} \tag{20}$$

which can be solved using well known convex optimization approaches. The typical form of the measurement operators, in the case of bipartite states, such as for signal ( $s$ ) and idler ( $i$ ) photons, is:

$$M_n = \Pi_j^s \otimes \Pi_k^i. \tag{21}$$

The problem reduces to constructing local operators  $\Pi_j^{s,i}$ . For the case a bipartite state given by Eq. (1) written in the OAM basis, it is apparent that the natural set of operators  $\Pi_j^{s,i}$ , are projectors in the OAM basis, of the form:

$$\Pi_j^{s,i} = |l_j\rangle\langle l_j|^{s,i}, \tag{22}$$

or suitably engineered linear combinations thereof [36]. This idea gives useful and practically tight bounds to the entanglement content, without assuming any prior knowledge about the state

nor its properties, such as its purity. If the set of expectation values  $\{\text{Tr}(M_n \hat{\rho})\}$  is tomographically complete, of course the Entanglement Witness gives the exact value. In practice, a much smaller number of measurements should be sufficient to arrive at reasonable bounds. The approach presented here is suitable for any finite-dimensional system, as long as the observables  $M_i$  are bounded operators.

#### 4. Proposed experimental implementation

The proposed experiment to demonstrate high-dimensional angular interference and entanglement using  $N$  angular slits is depicted in Fig. 1(a), and it is based on the standard experimental setups described for instance in Refs. [19,23]. In the setup described in Fig. 1(a) the pump is a Gaussian laser beam with zero OAM prepared by filtering the laser beam by using single mode fibers (SMFs). Typical power of the pump beam is in the range of 100 mW and typical operational wave-length is 413 nm. Down-converted photons with degenerate wavelength  $\lambda = 826$  nm are produced by the non-linear process of Spontaneous Parametric Down Conversion (SPDC). To this end, the Gaussian pump beam is normally incident on a non-linear crystal (typically  $\beta$ -barium borate (BBO)), phase matched either for type-I or type-II down-conversion. For the given pump beam and phase-matching parameters, conservation of OAM is granted by SPDC process [23]. The main novel ingredient introduced in the experimental setup depicted in Fig. 1(a) is given by the angular masks containing  $N$  and  $M$  angular slits for signal and idler photons, respectively, which can be programmed using standard Spatial Light Modulators (SLMs).

Angular aperture masks are placed in the path of signal and idler down-converted photons, produced by a pump beam with a Gaussian profile with zero OAM ( $l = 0$ ), as depicted in Fig. 1. The generated OAM spectrum transmitted through the angular apertures is analyzed in terms of transmitted spiral harmonics, typically over a range from  $l = -12$  to  $l = 12$ , by means of additional diffraction holograms. We stress that, in addition to the angular apertures, diffraction holograms are indeed required in order to analyze the OAM spectrum, and perform the required projection measurements. These projection measurements are required to demonstrate high-dimensional interference effects, which are detected via Coincidence Counts ( $R_{s,i}$ ), in the  $(l_s, l_i)$  OAM basis (see Fig. 1(c) for further reference).

Standard Spatial Light Modulators (SLMs) are used both for preparing the state via the angular apertures, and for analysing the resulting modes via diffraction holograms [19] (Fig. 1(c)). As it is well known in the literature [19], SLMs are programmable refractive elements, which enable full control of the amplitudes of the diffracted beams. In the standard technique, if the index of the analysis  $l$ -forked hologram is opposite to that of the incoming mode, planar wave-fronts with on-axis intensity are generated in the first diffraction order. The on-axis intensity can be coupled to single-mode fibers with high efficiency, and can be measured with single-photon detectors  $D_{s,i}$ , using a coincidence count circuit (see Fig. 1(a) for details).

The maximum number of angular slits  $N$ , and possible paths  $D = N^2$ , that can be implemented in an experimental setup as described in Fig. 1(a) will be fundamentally limited by the finite spatial and angular correlation width of signal and idler photons, as well as by the resolution of the Spatial Light Modulator (SLM) itself. While the correlation width of down-converted photons will be *limited* by the waist of the Gaussian pump beam  $w$ , among other parameters such as crystal width or photon-emission angle [41], the resolution of the SLM will be determined by the SLM pixel pitch ( $d$ ). We can make a very rough estimate of the maximum number of angular slits  $N$  by considering  $w = 300\mu\text{m}$  and  $d = 3.74\mu\text{m}$ , we can very roughly estimate the maximum number of angular slits  $N$  to be of order  $N \approx w/d \approx 80$ .

We note that the maximum number of angular slits that can be implemented will be fundamentally limited by the angular correlation width ( $\delta\phi$ ) of the two photons. Typical angular correlations width reported in the literature are below 1 degree ( $\delta\phi < 1^\circ$ ) [41]. We note however that  $\delta\phi$  can be tuned by tailoring the width of the crystal or the photon-emission angle [41].

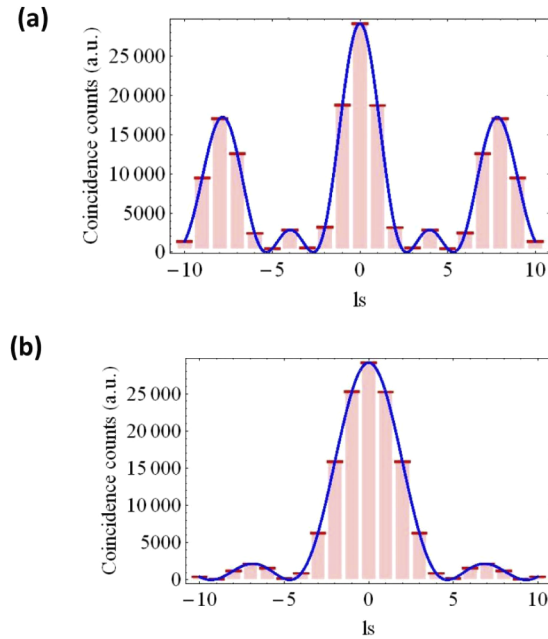


**Fig. 8.** Coincidence Count Rate ( $R_{s,i}$ ) given by Eq. (13) for pure non-maximally entangled states produced by imperfect phase-matching in combination with asymmetric slit configuration [24], as a function of  $l_s$ , for  $l_i = 0$ ,  $\alpha = \pi/10$ , off diagonal elements  $\rho_{nm} = \frac{1}{\sqrt{NM}} e^{i\theta}$ ,  $N = 6$  and  $M = 3$  angular slits. We consider different slit separations (a)  $\beta = \pi/4$ , (b)  $\beta = \pi/7$ . Such interference effects are a signature of non-maximal path entanglement in a  $D$ -dimensional space spanned by the different path alternatives of dimension  $D = N \times M = 18$ . As expected the period of the interference pattern decreases as  $\beta$  increases (see text for details).

Finally, we note that the attainable dimensionality in our system will be limited due to pixelation effects, leading to aliasing and diffraction which, in turn, introduces huge loss of visibility and could potentially prevent the detection of Entanglement Witnesses at such high dimensions.

## 5. Discussion

Higher dimensional entangled states are a fundamental resource both from the foundations of quantum mechanics perspective and for the development of new protocols in quantum communication. Maximally entangled states of bipartite quantum systems in an  $N$ -dimensional Hilbert space, the so called qudits, can introduce higher violations of local realism than qubits [42], and can prove more resilient to noise than qubits [42,43]. In quantum cryptography [44], or other quantum information protocols [36,45–49], use of entangled qutrits ( $N = 3$ ) [50,51] or qudits [52,53] instead of qubits is more secure against attacks. Moreover, it is known that quantum protocols work best for maximally entangled states. These facts motivate the development of techniques to generate maximally entangled states in higher dimensional Hilbert spaces. Entangled qutrits with two photons using an unbalanced 3-arm fiber optic interferometer [54] has been demonstrated. Time-bin entangled qudits up to  $D = 11$  from pump pulses generated by a mode-locked laser has also been reported [55]. Here we report a protocol that can produce entangled angular qudits based on angular diffraction. Our results suggest that such angular qudit states could possibly be suited for experimental demonstrations of violations of Bells inequalities in high dimensions, among other relevant applications.

## Appendix. Angular interference for $N=2$ angular slits

As a starting point, we reproduce the results reported in Jha *et al.* PRL2010 [23], for  $N = 2$  angular slits, resulting in  $N^2 = 4$  alternative pathways. The interference between the alternative paths manifests itself in the periodic dependence of the Coincidence Count Rate  $R_{si}$ , on the angular separation  $\beta$  and on the sum of OAMs  $l$ . We consider  $l_i = -2, 0, 2$ ,  $\alpha = \pi/10$ ,  $\beta = \pi/4, \pi/6, \pi/2, \pi$ , and a reported visibility  $V = 0.875$  [23]. In Fig. 7, we present a numerical simulation of Coincidence Count Rate  $R_{si}$ , given by Eq. (7) for  $\alpha = \pi/10$ ,  $\beta = \pi/4$  and  $L = 10$ . The width of the diffraction envelope increases as the angular aperture  $\alpha$  decreases, since angular position and OAM are Fourier related [16,17]. Therefore the uncertainty in OAM ( $\Delta l$ ) increases as the uncertainty in angular position ( $\Delta\phi$ ) decreases. Figure 7(a) and 7(b) correspond to  $l_i = 2$  and  $l_s = -2$ , respectively. Due to correlations in OAM of twin photons, the interference pattern is peaked at  $l_s = -l_i$ .

In Fig. 7(c) to 7(f), we present Coincidence Count Rates  $R_{si}$  given by Eq. (7), as a function of  $l_s$  for  $l_i = 0$ , and different values of slit separation  $\beta$ . We consider  $N = 2$ ,  $\alpha = \pi/10$ , and a reported visibility  $V = 0.875$  [23]. More specific, Fig. 7(c)  $\beta = \pi/6$ , Fig. 7(d)  $\beta = \pi/4$ , Fig. 7(e)  $\beta = \pi/2$ , Fig. 7(f)  $\beta = \pi$ . As expected the period of the interference pattern decreases as  $\beta$  increases (see Eq. (8)). Our numerical results perfectly reproduce the experimental results presented in Jha *et al.* PRL 2010, which further validates our analytical model.

## Funding

Secretaría de Ciencia y Técnica, Universidad de Buenos Aires (PDE 2017); Ministerio de Ciencia, Tecnología e Innovación Productiva (PICT STARTUP 2015 0710); ERDF (1.1.1.5/19/A/003).

## Acknowledgements

The author acknowledges Carlos Monken, Sonja Franke-Arnold, Leonardo Neves, and Giacomo Sorelli for helpful discussions. GP acknowledges J. Eisert for valuable insights into Entanglement Witnesses and convex optimization protocols.

## Disclosures

The author declares no conflicts of interest.

## References

1. C. K. Hong, Z. Y. Ou, and L. Mandel, "Measurement of subpicosecond time intervals between two photons by interference," *Phys. Rev. Lett.* **59**(18), 2044–2046 (1987).
2. T. J. Herzog, J. G. Rarity, H. Weinfurter, and A. Zeilinger, "Frustrated two-photon creation via interference," *Phys. Rev. Lett.* **72**(5), 629–632 (1994).
3. K. Jha, M. N. O'Sullivan, K. W. Clifford Chan, and R. W. Boyd, "Temporal coherence and indistinguishability in two-photon interference effects," *Phys. Rev. A* **77**(2), 021801 (2008).
4. J. Brendel, N. Gisin, W. Tittel, and H. Zbinden, "Pulsed Energy-Time Entangled Twin-Photon Source for Quantum Communication," *Phys. Rev. Lett.* **82**(12), 2594–2597 (1999).
5. R. Thew, S. Tanzilli, W. Tittel, H. Zbinden, and N. Gisin, "Experimental investigation of the robustness of partially entangled qubits over 11 km," *Phys. Rev. A* **66**(6), 062304 (2002).
6. E. J. S. Fonseca, P. H. Souto Ribeiro, S. Pádua, and C. H. Monken, "Quantum interference by a nonlocal double slit," *Phys. Rev. A* **61**(2), 023801 (2000).
7. N. Leonardo, G. Lima, J. G. Aguirre Gómez, C. H. Monken, C. Saavedra, and S. Pádua, "Generation of Entangled States of Qudits using Twin Photons," *Phys. Rev. Lett.* **94**(10), 100501 (2005).
8. N. Leonardo, G. Lima, E. J. S. Fonseca, L. Davidovich, and S. Pádua, "Characterizing entanglement in qubits created with spatially correlated twin photons," *Phys. Rev. A* **76**(3), 032314 (2007).
9. A. Aspect, P. Grangier, and G. Roger, "Experimental Realization of Einstein-Podolsky-Rosen-Bohm Gedankenexperiment: A New Violation of Bell's Inequalities," *Phys. Rev. Lett.* **49**(2), 91–94 (1982).
10. L. Mandel, *Rev. Mod. Phys.* **71**, <https://journals.aps.org/rmp/abstract/10.1103/RevModPhys.71.S274>, S274 (1999).
11. A. K. Ekert, "Quantum cryptography based on Bell's theorem," *Phys. Rev. Lett.* **67**(6), 661–663 (1991).
12. A. Zeilinger, "Experiment and the foundations of quantum physics," *Rev. Mod. Phys.* **71**(2), S288–S297 (1999).

13. C. H. Bennett and S. J. Wiesner, "Communication via one- and two-particle operators on Einstein-Podolsky-Rosen states," *Phys. Rev. Lett.* **69**(20), 2881–2884 (1992).
14. S. M. Barnett and D. T. Pegg, "Quantum theory of rotation angles," *Phys. Rev. A* **41**(7), 3427–3435 (1990).
15. C. H. Bennett, G. Brassard, C. Crépeau, R. Jozsa, and A. Peres, "Teleporting an unknown quantum state via dual classical and Einstein-Podolsky-Rosen channels," *Phys. Rev. Lett.* **70**(13), 1895–1899 (1993).
16. S. Franke-Arnold, S. M. Barnett, E. Yao, J. Leach, J. Courtial, and M. Padgett, "Uncertainty principle for angular position and angular momentum," *New J. Phys.* **6**, 103 (2004).
17. B. Jack, M. Padgett, and S. Franke-Arnold, "Angular Diffraction," *New J. Phys.* **10**(10), 103013 (2008).
18. A. K. Jha, B. Jack, E. Yao, J. Leach, R. W. Boyd, G. S. Buller, S. M. Barnett, S. Franke-Arnold, and M. J. Padgett, "Fourier relationship between the angle and angular momentum of entangled photons," *Phys. Rev. A* **78**(4), 043810 (2008).
19. A. Vaziri, G. Weihs, and A. Zeilinger, "Experimental Two-Photon, Three-Dimensional Entanglement for Quantum Communication," *Phys. Rev. Lett.* **89**(24), 240401 (2002).
20. J. Leach, B. Jack, J. Romero, M. Ritsch-Marté, R. W. Boyd, A. K. Jha, and S. M. Barnett, "Violation of a Bell inequality in two-dimensional orbital angular momentum state-spaces," *Opt. Express* **17**(10), 8287 (2009).
21. A. C. Dada, J. Leach, G. S. Buller, M. J. Padgett, and E. Andersson, "Experimental high-dimensional two-photon entanglement and violations of generalised Bell inequalities," *Nat. Phys.* **7**(9), 677–680 (2011).
22. P. G. Mattle, K. Weinfurter, H. Zeilinger, A. Sergienko, A. V. Shih, and Y. Kwiat, "New High-Intensity Source of Polarization-Entangled Photon Pairs," *Phys. Rev. Lett.* **75**(24), 4337–4341 (1995).
23. A. Kumar Jha, J. Leach, B. Jack, S. Franke-Arnold, S. Barnett, R. Boyd, and M. Padgett, "Angular Two-Photon Interference and Angular Two-Qubit States," *Phys. Rev. Lett.* **104**(1), 010501 (2010).
24. P. Machado, A. A. Matoso, M. R. Barros, L. Neves, and S. Padua, "Engineering quantum correlations for  $m \times n$  spatially encoded two-photons states," *Phys. Rev. A* **99**(6), 063839 (2019).
25. G. Sorelli, V. N. Shatokhin, and A. Buchleitner, "Universal entanglement loss induced by angular uncertainty," *J. Opt.* **22**(2), 024002 (2020).
26. A. Vaziri, G. Weihs, and A. Zeilinger, "Experimental Two-Photon, Three-Dimensional Entanglement for Quantum Communication," *Phys. Rev. Lett.* **89**(24), 240401 (2002).
27. M. N. O'Sullivan-Hale, I. A. Khan, Robert W. Boyd, and John C. Howell, "Pixel Entanglement: Experimental Realization of Optically Entangled  $d=3$  and  $d=6$  Qudits," *Phys. Rev. Lett.* **94**(22), 220501 (2005).
28. S. Ramelow, L. Ratschbacher, A. Fedrizzi, N. K. Langford, and A. Zeilinger, "Discrete Tunable Color Entanglement," *Phys. Rev. Lett.* **103**(25), 253601 (2009).
29. J. G. Rarity and P. R. Tapster, "Experimental violation of Bell's inequality based on phase and momentum," *Phys. Rev. Lett.* **64**(21), 2495–2498 (1990).
30. B. Jack, J. Leach, H. Ritsch, S. M. Barnett, M. J. Padgett, and S. Franke-Arnold, "Precise quantum tomography of photon pairs with entangled orbital angular momentum," *New J. Phys.* **11**(10), 103024 (2009).
31. G. Puentes, D. Voigt, A. Aiello, and J. P. Woerdman, "Tunable spatial decoherers for polarization-entangled photons," *Opt. Lett.* **31**(13), 2057–2059 (2006).
32. A. Ling, P. Y. Han, A. Lamas-Limaes, and C. Kurtsiefer, "Preparation of Bell state with controlled white noise," *Laser Phys.* **16**(7), 1140–1144 (2006).
33. T-C Wei, J. B. Altepeter, D. Branning, P. M. Goldbart, D. F. James, E. Jeffrey, P. G. Kwiat, S. Mukhopadhyay, and N. Peters, "Synthesizing arbitrary two-photon mixed states," *Phys. Rev. A* **71**(3), 032329 (2005).
34. W. K. Wootters, "Entanglement of Formation of an Arbitrary State of Two Qubits," *Phys. Rev. Lett.* **80**(10), 2245–2248 (1998).
35. P. Rungta, V. Bužek, C. M. Caves, M. Hillery, and G. J. Milburn, "Universal state inversion and concurrence in arbitrary dimensions," *Phys. Rev. A* **64**(4), 042315 (2001).
36. G. Puentes, A. Datta, A. Feito, J. Eisert, M. B. Plenio, and I. A. Walmsley, "Entanglement quantification from incomplete measurements: applications using photon-number-resolving weak homodyne detectors," *New J. Phys.* **12**(3), 033042 (2010).
37. K. M. R. Audenaert and M. B. Plenio, "When are correlations quantum?—verification and quantification of entanglement by simple measurements," *New J. Phys.* **8**(11), 266 (2006).
38. J. Eisert, F. G. S. L. Brandão, and K. M. R. Audenaert, "Quantitative entanglement witnesses," *New J. Phys.* **9**(3), 46 (2007).
39. M. B. Plenio, "Logarithmic Negativity: A Full Entanglement Monotone That is not Convex," *Phys. Rev. Lett.* **95**(9), 090503 (2005).
40. R. Bhatia, *Matrix analysis*, (Springer, 1997).
41. M. Jost Bradley, V. Sergienko Alexander, F. Abouraddy Ayman, Bahaa E. A. Saleh, and C. Teich Malvin, "Spatial correlations of spontaneously down-converted photon pairs detected with a single-photon-sensitive CCD camera," *Opt. Express* **3**(2), 81 (1998).
42. D. Collins, N. Gisin, N. Linden, S. Massar, and S. Popescu, "Bell Inequalities for Arbitrarily High-Dimensional Systems," *Phys. Rev. Lett.* **88**(4), 040404 (2002).
43. D. Kaszlikowski, P. Gnaniński, M. Żukowski, W. Miklaszewski, and A. Zeilinger, "Violations of Local Realism by Two Entangled N-Dimensional Systems Are Stronger than for Two Qubits," *Phys. Rev. Lett.* **85**(21), 4418–4421 (2000).

44. H. Bechmann-Pasquinucci and A. Peres, "Quantum Cryptography with 3-State Systems," *Phys. Rev. Lett.* **85**(15), 3313–3316 (2000).
45. G. Puentes, G. Waldherr, P. Neumann, G. Balasubramanian, and J. Wrachtrup, "Efficient route to high-bandwidth nanoscale magnetometry using single spins in diamond," *Sci. Rep.* **4**(1), 4677 (2015).
46. G. Puentes, A. Aiello, D. Voigt, and J. P. Woerdman, "Maximally entangled mixed-state generation via local operations," *Phys. Rev. A* **75**(3), 032319 (2007).
47. G. Puentes, G. Colangelo, R. J. Sewell, and M. W. Mitchell, "Planar squeezing by quantum non-demolition measurement in cold atomic ensembles," *New J. Phys.* **15**(10), 103031 (2013).
48. O. Takayama, J. Sukham, R. Malureanu, A. V. Lavrinenko, and G. Puentes, "Photonic spin Hall effect in hyperbolic metamaterials at visible wavelengths," *Opt. Lett.* **43**(19), 4602–4605 (2018).
49. S. Moulieras, M. Lewenstein, and G. Puentes, "Entanglement engineering and topological protection by discrete-time quantum walks," *J. Phys. B: At., Mol. Opt. Phys.* **46**(10), 104005 (2013).
50. A. K. Ekert, "Quantum cryptography based on Bell's theorem," *Phys. Rev. Lett.* **67**(6), 661–663 (1991).
51. M. Bourennane, A. Karlsson, and G. Bjork, "Quantum key distribution using multilevel encoding," *Phys. Rev. A* **64**(1), 012306 (2001).
52. T. Durt, N. J. Cerf, N. Gisin, and M. Zukowski, "Security of quantum key distribution with entangled qutrits," *Phys. Rev. A* **67**(1), 012311 (2003).
53. N. J. Cerf, M. Bourennane, A. Karlsson, and N. Gisin, "Security of Quantum Key Distribution Using d-Level Systems," *Phys. Rev. Lett.* **88**(12), 127902 (2002).
54. R. T. Thew, A. Acin, H. Zbinden, and N. Gisin, "Bell-Type Test of Energy-Time Entangled Qutrits," *Phys. Rev. Lett.* **93**(1), 010503 (2004).
55. A. Vaziri, G. Weihs, and A. Zeilinger, "Experimental Two-Photon, Three-Dimensional Entanglement for Quantum Communication," *Phys. Rev. Lett.* **89**(24), 240401 (2002).